Validation of CFD determined hydrodynamic coefficients for a semisubmersible floating offshore wind turbine

Ramesh Reddy, Likhitha; Milano, Daniel; Walker, John; Vire, Axelle

Important note
To cite this publication, please use the final published version (if applicable).
Please check the document version above.

PAPER • OPEN ACCESS

Validation of CFD determined hydrodynamic coefficients for a semisubmersible floating offshore wind turbine

View the article online for updates and enhancements.

Validation of CFD determined hydrodynamic coefficients for a semisubmersible floating offshore wind turbine

Likhitha Ramesh Reddy[1], Daniel Milano[2], John Walker[2], Axelle Viré[1]

[1]Faculty of Aerospace Engineering, Delft University of Technology, Delft, Netherlands
[2]Offshore Renewable Energy Catapult, Glasgow, UK

E-mail: l.rameshreddy@tudelft.nl

Abstract. The hydrodynamic characteristics are crucial for accurately analysing floating offshore wind systems. In this paper, the added mass and damping coefficients of a semisubmersible floater are examined around the natural periods of the surge, heave, and pitch motion, using computational fluid dynamics (CFD). The OpenFOAM CFD setup is validated against experimental measurements from the free decay tests, and the same setup is used to determine the hydrodynamic coefficients of the platform subjected to forced motions with different amplitudes and periods. The added mass and quadratic damping coefficients obtained from forced oscillations are consistent with the free decay results. Moreover, the added mass coefficients obtained by CFD is significantly higher than the estimations of the potential flow theory: around 10% larger for surge and 22% larger for heave. The damping is almost independent of the frequency while it varies with the motion amplitude. The deviations in the CFD results from the potential flow theory are due to the viscous effects. Besides, viscous damping is dependent on the drag coefficient specified in the Morison's equation .

Keywords: semi-submersible, added mass, damping coefficient, floating offshore wind turbines, forced oscillations

1. Introduction

Floating Offshore Wind Turbines (FOWTs) have gained increasing attention in recent years due to their significant potential to harness wind energy in deep-water offshore regions. The current study focuses on the "DeepCwind" semisubmersible FOWT, which comprises four cylindrical columns connected by a set of braces, which is defined by Robertson et al. [1]. One of the critical design aspects is the accurate prediction of hydrodynamic loading on the substructures, necessary for the precise estimation of the Fatigue Limit State (FLS) and Ultimate Limit State (ULS) to ensure a safe design of the floater.

Most modelling approaches are based on the potential flow theory, Morison's equation, or a combination of both. The OC5 (Offshore Code Comparison Collaboration Continuation, with Correlation) campaign showed that these tools consistently under-predicted the hydrodynamic loading (by about 20%) as these models are limited to linear or weakly non-linear analysis [2]. Furthermore, the semisubmersible design incorporates heave plates attached to the base of its columns to reduce the heave motion by providing supplementary added mass, and viscous damping from flow separation and vortex shedding[3]. These factors call for high fidelity simulation tools that accurately capture non-linear hydrodynamics including viscous effects, thereby correctly estimating the added mass and damping coefficients.

Hydrodynamic coefficients are characterised by motion amplitude and frequency (period). Keulegan-Carpenter (KC) number and Stokes number β (or Reynolds number Re) are the corresponding non-dimensional parameters. In the calm water, they are defined as:

$$KC = \frac{2\pi A}{D}, \text{ for surge and heave motion}; KC = 2\pi\theta_0, \text{ for pitch motion} \tag{1}$$

$$\beta = \frac{D^2}{\nu T} = \frac{Re}{KC} \tag{2}$$

CFD analysis of the semisubmersible

where A is the motion amplitude for surge and pitch, θ_0 is the pitch motion amplitude, D is the characteristic length (diameter of each column), ν is the kinematic viscosity of water, and T is the time period of motion.

Many experimental studies have investigated the effect of these parameters on hydrodynamic coefficients. Cozijn et al. [4] performed forced oscillation tests of the CALM buoy in heave, roll, and pitch and found that the linear radiation-diffraction calculations underestimated the added mass. Wadhwa et al. [5] examined the dependence of the hydrodynamic response with motion amplitude for a fixed oscillation frequency, identifying a critical KC value above which the added mass coefficient showed non-linear amplitude dependence. Lopez-pavon et al. [6] investigated the heave plates of the semisubmersible platform for KC values ranging from 0.3-0.9. The resulting hydrodynamic coefficients showed dependence on the KC number and have insignificant dependence on the oscillation period. Furthermore, Nallayarasu et al. [7], Philip et al. [8], and others confirmed the high amplitude dependency and weak frequency dependency at low KC values.

In addition to the experimental studies, Lopez-pavon et al. [6] computed the hydrodynamic coefficients with a commercial CFD software, ANSYS-CFX, and the results agreed well with the experiments. Zhang et al. [9] performed large-eddy simulations to examine the hydrodynamic coefficients of multiple heave plates. These numerical studies used forced oscillation tests to determine the added mass and damping coefficients. However, free decay simulations can also be used to estimate these parameters as demonstrated by Burmester et al. [10].

Most of the research done in this area focused on a single-cylinder attached to thin heave plates, which is a different configuration than that of "DeepCwind" semisubmersible as it contains thicker heave plates. Furthermore, most studies often neglect the influence of other columns and braces. In this paper, added mass and damping coefficients are extracted by performing CFD simulations at different KC and β. These results are compared to the linear potential-flow solution obtained from the commercial solver WAMIT. The current study focuses on how these hydrodynamic parameters are computed using CFD. This task requires a CFD setup defined in Section 2 and validated in Section 3, which is used to perform forced oscillation simulations of the semisubmersible in surge, heave and pitch. Further, added mass and damping coefficients are obtained using the Fourier-averaged method (Section 4). Results are discussed in Section 5, and conclusions are drawn in Section 6.

2. Numerical Modelling

High-fidelity simulations are performed using OpenFOAM-v2012, an open-source CFD toolbox. The interFoam solver (also referred to as interDyMFoam in earlier versions of OpenFOAM) is a multiphase fluid-structure interaction solver that solves the Navier-stokes equations coupled with 6 degrees-of-freedom (DOF) rigid-body equations of motion.

2.1. Governing Equations

The fluid flow can be represented by the following incompressible Reynolds-averaged Navier-Stokes equations, as both air and water are considered as incompressible Newtonian fluids.

$$\nabla \cdot \mathbf{u} = 0 \tag{3}$$

$$\frac{\partial \rho \mathbf{u}}{\partial t} + \nabla \cdot (\rho \mathbf{u}\mathbf{u}) = -\nabla p + \mathbf{F_b} + \nabla \cdot \boldsymbol{\tau},$$

$$\text{with} \quad \boldsymbol{\tau} = (\mu + \mu_t)(\nabla \mathbf{u} + (\nabla \mathbf{u})^T) - \frac{2}{3}\rho k \mathbf{I} \tag{4}$$

where $\mathbf{u}$ is the flow velocity vector, p is the pressure, $\mathbf{F_b}$ is the body forces term, μ is the dynamic viscosity, ρ denotes the local fluid density, and $\boldsymbol{\tau}$ is the viscous stress tensor. μ_t, and k are turbulence eddy viscosity and turbulent kinetic energy, respectively, which is modelled using k-omega Shear Stress Transport (SST) formulation [10].

The air-water interface is tracked using the volume of fluid (VOF) method [11]. The free surface is tracked by the a volume fraction of water, α. $\alpha \in [0, 1]$, where α=0 represents all air and α=1 is all water. The cells where $0 < \alpha < 1$ contain the air-water interface. The volume fraction is given by the

CFD analysis of the semisubmersible

advection equation:

$$\frac{\partial \alpha}{\partial t} + \nabla \cdot (\mathbf{u}\alpha) + \nabla \cdot (\mathbf{u_r}\alpha(1-\alpha)) = 0 \tag{5}$$

where $\mathbf{u_r}$ is the compression velocity, and the last term of Equation 5 is an artificial compression term [12] that counteracts the numerical diffusion in the interface zone. The density ρ and the dynamic viscosity μ in each cell are then given by:

$$\rho = \alpha\rho_{water} + (1-\alpha)\rho_{air} \tag{6}$$

$$\mu = \alpha\mu_{water} + (1-\alpha)\mu_{air} \tag{7}$$

2.2. CFD setup

2.2.1. Computational Domain and Boundary Conditions
The computational domain, along with the boundaries, is shown in Figure 1a. All the simulations are carried out at a 1:50 model scale. The dimensions of the rectangular fluid domain are defined according to the specifications mentioned by Wang et al. [13]. The boundary conditions, along with the boundary locations specified in OpenFOAM, are described in Table 1. While the floater displacement is calculated based on the total forces in free decay load cases, a sinusoidal displacement (surge, heave or pitch motion) is applied in forced oscillations. For the volume fraction function, setFields utility is used to specify the initial conditions, with $\alpha = 1$ in the region bounded by $-200 \leq x \leq 200, -100 \leq y \leq 100, -180 \leq z \leq 0$, and $\alpha = 0$ elsewhere. The simulations are performed without relaxation zones, and they yield similar results to those achieved with relaxation zones.
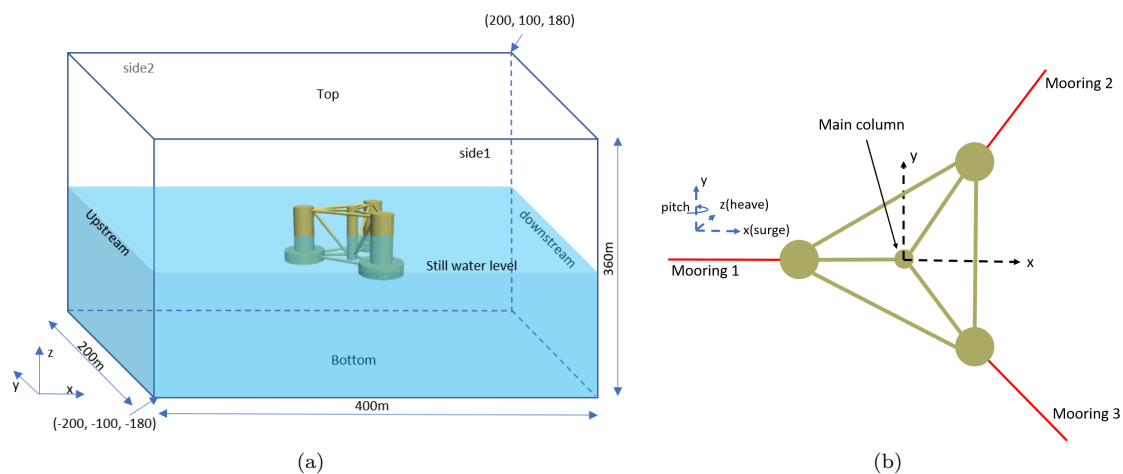

Figure 1: a) Computational domain with domain dimensions (in full scale); b) Three Taut spring mooring lines. In the case of free decay simulations, mooring lines are defined as linear springs, whereas they are not defined in forced oscillation tests

2.2.2. Computational Grid
The computational mesh was generated within OpenFOAM using the blockMesh utility to create a background mesh. Further, the snappyHexMesh tool refined the mesh closer to the floater. The refinement zones are consistent with the recommendations by Wang et al. [13]. Figure 2 displays the very fine resolution near the corner of the heave plates and the bottom of the main column to capture the flow separation phenomenon. In addition, prism layers were added to capture the wall boundary layer [13].

2.2.3. Numerical Schemes
The Courant-Friedrichs-Lewy (CFL) condition is imposed for the temporal discretisation. Therefore, the time step is set to run-time adjustable to maintain a maximum Courant number of 1.0. The

CFD analysis of the semisubmersible

Table 1: Boundary conditions and boundary locations in full scale specified in CFD simulations

| Boundary	Location	Boundary type	Velocity	Pressure	Volume fraction
Floater	NA	Wall	No slip	Fixed Flux	Zero Gradient
Upstream	x=−200m	Wall	Slip	Zero Gradient	Zero Gradient
Downstream	x=+200m	Wall	Slip	Zero Gradient	Zero Gradient
Top	y=+100m	Pressure Outlet	Pressure-inlet Outlet	Atmospheric pressure	Zero
Bottom	y=−100m	Velocity Inlet	Zero	Zero Gradient	Zero Gradient
sides	z=±180m	Wall	Slip	Zero Gradient	Zero Gradient
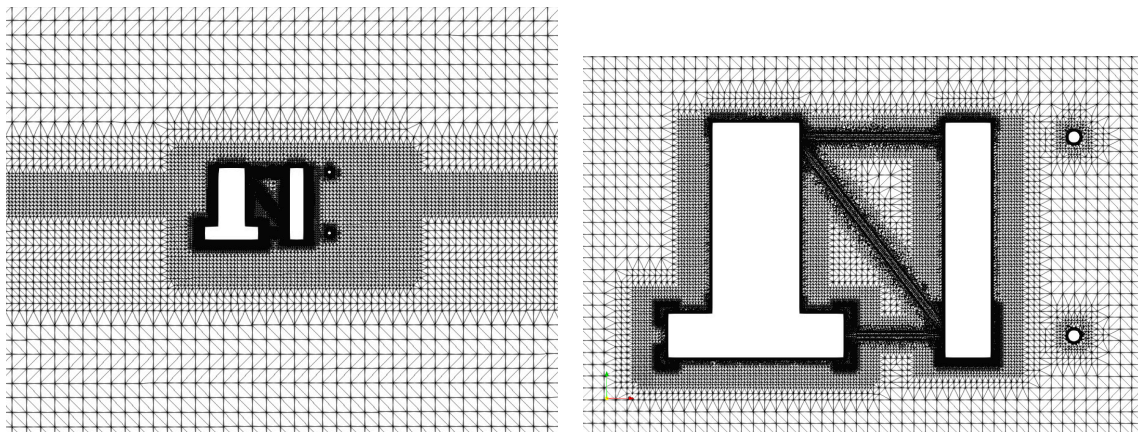
Figure 2: Computational grid arrangement and the refinement zones near the floater

numerical schemes and settings used are summarised in Table 2. Due to higher mesh non-orthogonality, limited schemes are used for Laplacian and surface normal gradient to improve numerical stability at the cost of reduced accuracy.

Table 2: Description of the numerical schemes and settings in OpenFOAM

Time scheme	Euler – first-order implicit, bounded
Gradient scheme	cellLimited Gauss linear, bounded
Divergence scheme	Gauss linear
Laplacian scheme	Gauss linear limited 0.33
Surface normal gradient scheme	limited corrected 0.33
Pressure-velocity coupling	PIMPLE Algorithm nCorrectors=3 nOuterCorrectors=1 nNonOrthogonalCorrectors=3
6-DOF solver	Newmark solver
Acceleration-relaxation factor	1.0
Interface capturing scheme	MULES algorithm Interpolation scheme: interface compression with VanLeer interpolation

A deforming mesh technique is implemented to comply with the floater's motion. For free decay simulations, innerDistance and outerDistance is specified in the solver. The mesh nodes inside the innerDistance displace with the floater as a rigid body, whereas the nodes between the innerDistance and outerDistance morph. The rest of the computational grid remains unmodified. However, in the case of forced oscillations, the solver utilises the inverse distance diffusivity function to govern the mesh

CFD analysis of the semisubmersible

morphing. The diffusivity function is defined as the square of the inverse distance between the floater and the mesh position; i.e., the mesh morphing decreases as the mesh element moves away from the floater [15].

For free decay simulations, the semisubmersible is restrained by the mooring lines (displayed in Figure 1b), which is defined as linear springs with constant stiffness in the simulations to be consistent with the experimental setup[14].

3. Experimental Validation of the CFD setup - Free Decay Simulations

Heave and pitch free decay simulations of the floater are carried out to determine the natural periods and damping. The results are validated with the experimental data, as a part of the OC6 project [13]. The details of heave and pitch free decay tests are specified in Table 3. Load cases 1.1 and 1.2 correspond to load cases 4.4 and 4.6 in [13]. The damping ratio ζ is calculated using logarithmic decrement δ from the response amplitude decay plot. The damping ratio and logarithmic decrement are defined as follows:

$$\zeta = \frac{1}{\sqrt{1 + (\frac{2\pi}{\delta})^2}} \tag{8}$$

$$\delta = log(\frac{x_n}{x_{n+1}}) \tag{9}$$

where x_n and x_{n+1} are amplitudes of two consecutive peaks or troughs.

Table 3: Free decay simulations: Load cases specifying floater initial offset and the natural periods

Load case	Full scale			Model scale		
	Initial offset	Period	Simulation Time	Initial offset	Period	Simulation Time
1.1-Heave	-2.1687m	17.2s	350s	-0.043374m	2.43s	49.5s
1.2-Pitch	-5.6719°	31.0s	450s	-5.6719°	4.39s	63.6s

The heave and pitch decaying motions are represented in Figure 3. In both cases, the experimental results and the CFD results match very closely initially, but in the later time periods, CFD results are highly damped. This discrepancy can be attributed to the choice of limited schemes in OpenFOAM, where the accuracy was comprised for numerical stability. Nonetheless, the natural periods are in good agreement with about $\pm 3.5\%$ error. The heave and pitch damping ratios are plotted in Figure 4. The heave damping ratio increases linearly with amplitude at smaller amplitudes and non-linearly at large amplitudes. The very high damping ratio at the larger amplitude can also result from the transient start-up effect and cannot be entirely attributed to amplitude dependency.

4. Forced Oscillation Simulations

As established earlier, forced oscillations in the surge, heave and pitch direction are carried out to identify the added mass and damping coefficients. In this simulation, a sinusoidal motion is imposed on the floater, which is given by Equation 10.

$$X(t) = A \sin(\omega t) \tag{10}$$

where $X(t)$ represents time-varying displacement in surge ($x(t)$), heave ($z(t)$), and pitch ($\theta(t)$), A is the oscillation amplitude, and ω is the angular frequency of the oscillation.

The load cases are specified in Table 4. A set of 27 simulations are performed, with KC numbers varying from 0.5 to 10 and β ranges between $2.5 \cdot 10^5$ and $5.8 \cdot 10^7$.
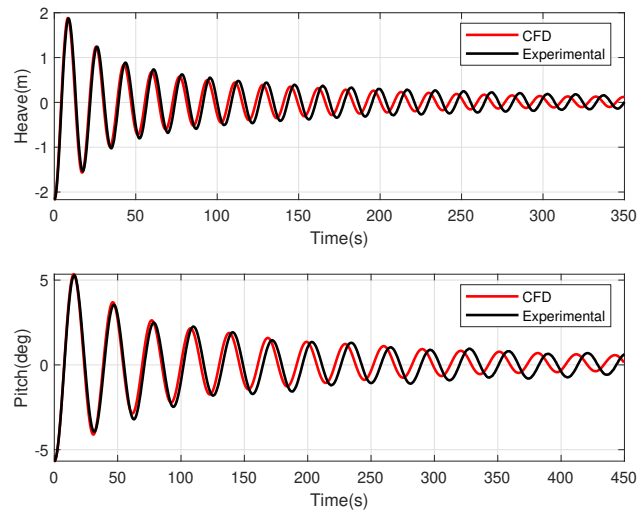
CFD analysis of the semisubmersible

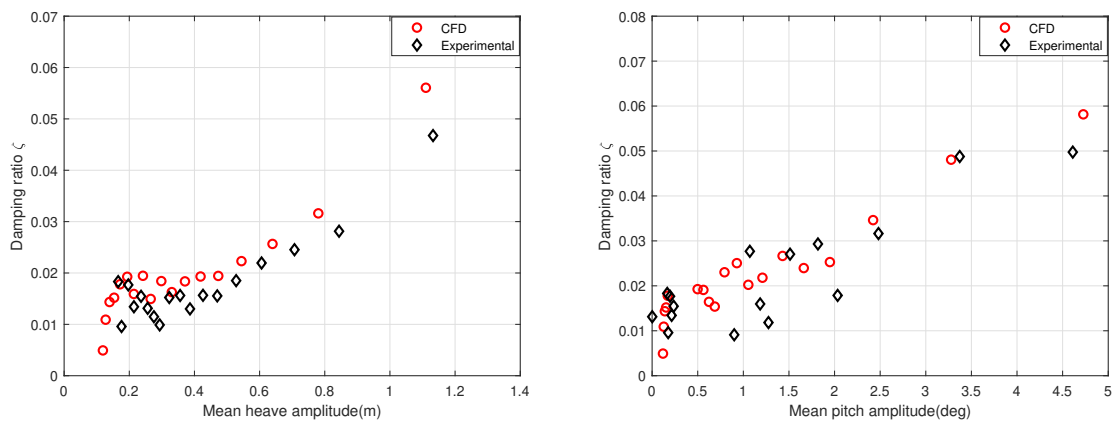Figure 3: Free decay simulations (top: decaying heave motion, bottom: decaying pitch motion)

Figure 4: Heave and pitch damping ratios obtained by free decay simulations

Table 4: Load cases for the forced oscillation tests

Surge forced oscillation		Heave forced oscillation		Pitch forced oscillation	
T(s)	A(m)	T(s)	A(m)	T(s)	A(deg)
	1.03		1.03		3.5
166	5.17	50	5.17	31	7.0
	10.34		7.5		12.5
	1.03		1.03		3.5
105	5.17	17.2	5.17	20	7.0
	10.34		7.5		12.5
	1.03		1.03		3.5
20	5.17	10	5.17	10	7.0
	10.34		7.5		12.5

4.1. Fourier Averaged Added Mass and Damping Coefficients

The added mass and damping coefficients are obtained from the time series of the hydrodynamic force, using the Fourier-averaged method. The hydrodynamic force on the floater, $F_H(t)$, is obtained by

CFD analysis of the semisubmersible

removing the hydrostatic restoring force, $F_K(t)$, and the radiation damping force, $F_R(t)$, from the total force exerted by the fluid on the structure, F(t).

$$F_H(t) = F(t) - F_K(t) - F_R(t) \tag{11}$$

$$F_K(t) = -CX(t) \tag{12}$$

$$F_R(t) = -C_r\dot{X}(t) \tag{13}$$

where, C is the hydrostatic stiffness, C_r is the radiation damping coefficient, and $\dot{X}(t)$ is the structural velocity. Radiation damping is negligible compared to viscous damping; thus, radiation damping force can be ignored to compute $F_H(t)$[13]. The hydrostatic restoring force $F_K(t)$ for surge, heave and pitch motions is given as:

$$F_K(t) = 0 \text{ in surge motion}; F_K(t) = \rho g A_w z(t) \text{ in heave motion}; F_K(t) = \rho g(VZ_b+I_y)\theta(t) \text{ in pitch motion} \tag{14}$$

Here, ρ is the water density, A_w is the waterplane area, V is the displaced volume of the floater, Z_b is the vertical coordinate of the center of buoyancy, and I_y is the waterplane area moment of interia about y axis.

From Equation 10, the structural velocity and acceleration are $\dot{X}(t) = A\omega cos(\omega t)$ and $\ddot{X}(t) = -A\omega^2 sin(\omega t)$. The hydrodynamic force expressed in the form of Morison's equation is given as:

$$F_H(t) = -\rho A\omega^2 C_a V sin(\omega t) - \frac{1}{2}\rho A_s A^2 \omega^2 C_{d_{x,z}} cos(\omega t)|cos(\omega t)| \tag{15}$$

The Morison equation does not apply to the pitch motion. However, the form of Equation 15 can be generalised to pitch motion. Thereby, the hydrodynamic moment can be given by:

$$M_H(t) = -A\omega^2 C_{Ia} I sin(\omega t) - \frac{1}{2}\rho A_s R A^2 \omega^2 C_\phi cos(\omega t)|cos(\omega t)| \tag{16}$$

where, A_s represents the projected area of the floater, I is the mass moment of inertia of the displaced water about y axis. Subsequently, using Equation 15 and Equation 16, the Fourier averaged coefficients is given as follows [16]:

$$C_a = \frac{1}{\pi\rho V\omega A}\int_0^T F_H(t)sin(\omega t)dt \quad \text{or} \quad C_{Ia} = \frac{1}{\pi\rho V D^2\omega A}\int_0^T M_H(t)sin(\omega t)dt \tag{17}$$

$$C_{d_{x,z}} = \frac{-3}{4\rho A_s\omega A^2}\int_0^T F_H(t)cos(\omega t)dt \quad \text{or} \quad C_\phi = \frac{-3}{4\rho A_s D\omega A^2}\int_0^T M_H(t)cos(\omega t)dt \tag{18}$$

where, C_a is the surge and heave added mass coefficient, C_{Ia} is the pitch added mass coefficient, $C_{d_{x,z}}$ represents the surge(x) and heave(z) quadratic damping coefficient, and C_ϕ is the pitch quadratic damping coefficient. Since Equation 16 is the generalised form of Equation 15, C_ϕ represents a parameter proportional to the quadratic pitch damping coefficient and does not signify the drag coefficient directly. As the objective of the paper is to understand the variation of these hydrodynamic coefficients with KC and β, this generalisation would not affect the observations made.

5. Results and Discussion

5.1. Forced Oscillations in Surge

The surge added mass and quadratic damping coefficients obtained by the CFD simulations are demonstrated in Figure 5. The CFD results are compared to the frequency-domain potential flow solution, combined with Morison's equation (will be referred to as potential flow solution from here on). From Figure 5, it is inferred that the surge added mass increases with the decreasing amplitude (or KC number) and increasing oscillation period. In addition, the results by Gao et al. [17] show that added mass is weakly dependent on KC number for $KC < 2$, while the added mass coefficient decreases with increasing KC at larger KC values. A similar trend is seen with surge added mass, where the added mass coefficients were similar at smaller amplitude (1.03m and 5.17m). Moreover, the potential flow results underestimate the surge added mass up to 9%.

CFD analysis of the semisubmersible

The CFD estimated surge quadratic damping coefficient decreases with increasing KC number and increases with the oscillation period. In contrast to added mass, the damping coefficient was weakly dependent on amplitude at a higher KC number ($KC > 3$), which conforms with the results of Dütsch et al. [18]. The potential flow solution underestimates the damping coefficient at lower KC. However, the results are close to the CFD simulations at larger KC numbers. To validate the forced oscillations results, the hydrodynamic coefficients were compared to the free decay tests performed by Wang et al. [13]. The time periods for different cycles are very close in the surge decaying motion, confirming the weak KC number dependency of the added mass (when KC is small). The damping calculated from free decay agrees well with the forced oscillations.
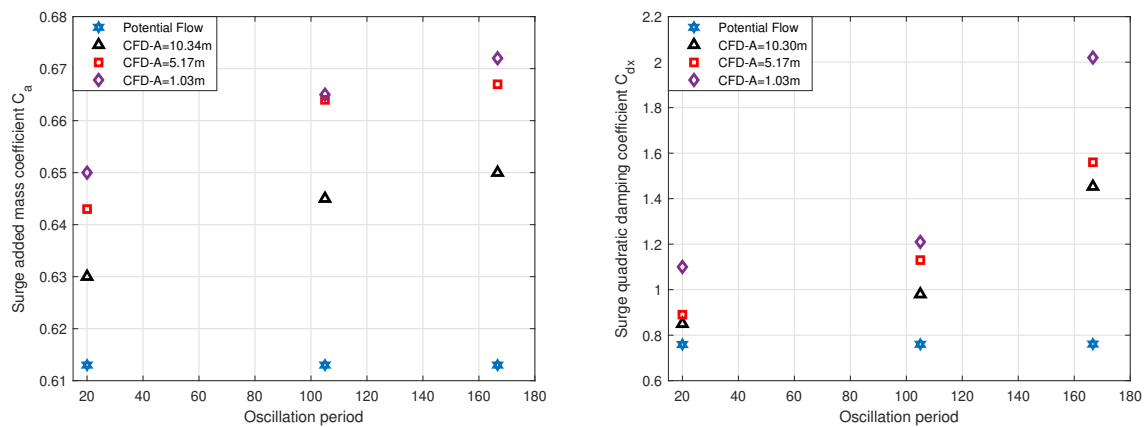

Figure 5: Surge added mass and damping coefficients

5.2. Forced Oscillations in Heave

Figure 6 shows the comparison between the CFD heave added mass and damping coefficient with the potential flow solution. The added mass coefficient increases with oscillation amplitude except at T=50s. Nevertheless, the difference between the added mass coefficient at A=5.17m and A=7.55m is negligible and can be attributed to numerical uncertainty. The added mass parameter does not follow a set-trend for small values of KC, but it appears to be weakly dependent on the oscillation period at higher KC values. Apart from this, the heave added mass is significantly higher (about 22%) at higher amplitudes than the potential flow solution. This can be credited to the increased flow separation at the edge of the heave plates at large floater motions as seen in other literature [4], [6].

The quadratic heave damping coefficient is independent of the oscillation period but decreases with increasing amplitude, which can be confirmed by Zhang et al. [9]. The heave plates induce vortex shedding, producing viscous damping that dominates in heave motion. Morison's equation models quadratic drag force using a constant drag coefficient, but due to the strong dependency of CFD determined damping on KC number, a single value of drag coefficient cannot correctly predict the heave damping in all cases. From Equation 18, quadratic damping coefficient is inversely proportional to the motion amplitude, which is confirmed by the damping ratio (Figure 4) estimated in free decay simulations.

5.3. Forced Oscillations in Pitch

A comparison of pitch added moment of inertia and quadratic damping computed from CFD and potential flow solution is represented in Figure 7. Overall, both these hydrodynamic parameters are underestimated by the potential flow solution. The pitch added mass coefficient weakly depends on amplitude while decreasing with the oscillation period at high pitch motions. These results do not conform well with published literature, where the pitch added mass coefficient increases as the oscillation period, contrary to the results obtained in this paper[15]. A possible reason might be the
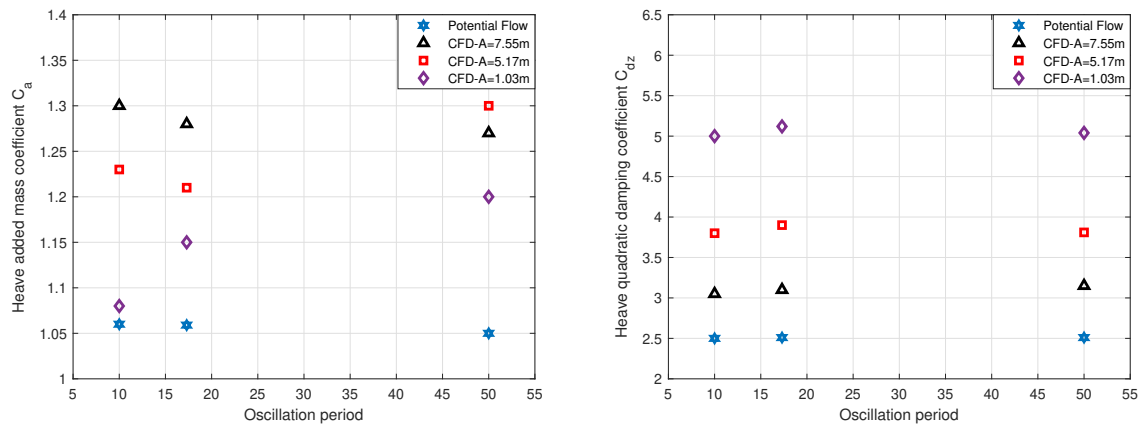
CFD analysis of the semisubmersible

Figure 6: Heave added mass and damping coefficients

complex vortex shedding pattern generated by large pitch motions. Another possible explanation is the numerical accuracy of the CFD results, which would require further investigation.

The quadratic pitch damping coefficient decreases with increasing KC number and is independent of the oscillation frequency, similar to the heave damping coefficient. Since viscous damping dominates in this case, the drag coefficients used by Morison's equation underpredict the viscous damping as a single drag coefficient cannot capture the frequency and amplitude dependency on these hydrodynamic coefficients. In the pitch free decay case, the damping ratios (Figure 4) increase with the pitch amplitude, contrary to the forced oscillation results. Moreover, the linear damping ratio increases linearly with pitch amplitude in the free decay case because of the presence of a constant quadratic damping coefficient. The linear damping ratio ζ is proportional to $C_{d_l} + A \cdot C_d$, where C_{d_l} is the linear damping coefficient.
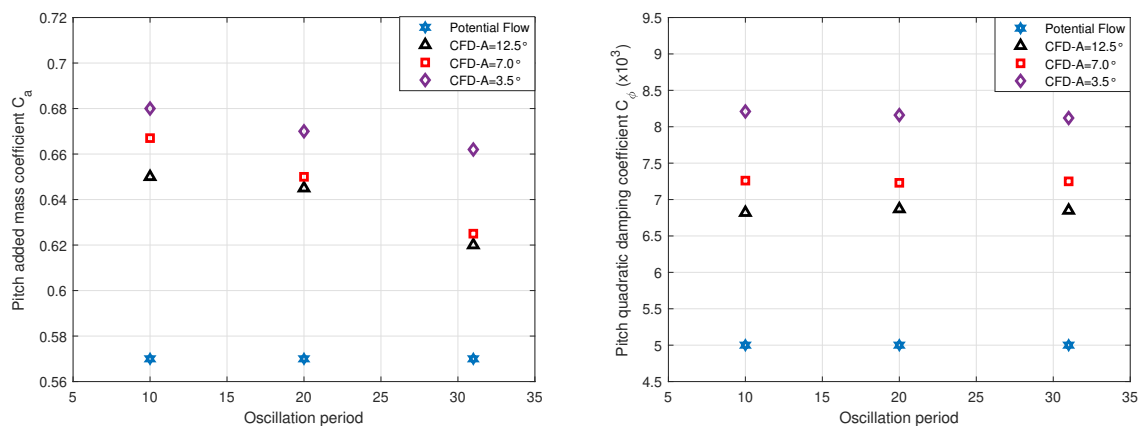

Figure 7: Pitch added mass and damping coefficients

6. Conclusions

The still-water hydrodynamic characteristics of a "DeepCwind" semisubmersible have been discussed in this paper. The CFD setup in OpenFOAM has been validated with experimental results by performing free decay simulations. In order to estimate the added mass and damping coefficient, a set of forced oscillation simulations have been conducted for a range of KC and β in the surge, pitch, and heave

CFD analysis of the semisubmersible

motion. Total forces have been recorded, from which these hydrodynamic parameters have been derived. The main findings can be summarised below:

- Both the added mass and damping coefficients showed small dependency on the frequency and, on the contrary, showed significant dependence on motion amplitude, which is coherent with previously published research.

- The potential flow solver combined with Morison's equation predominantly underestimates the added mass and damping coefficient for all the cases, which can be accredited to the dominating viscous effects. The accuracy of capturing the viscous damping using Morison's drag force is sensitive to the drag coefficient. The results also indicate that viscous correction to the added mass is also needed to more accurately capture the natural period of a floating structure.

- Surge added mass coefficient displays weak amplitude dependency at small amplitude and more extended periods. Moreover, surge added mass also demonstrates minor period dependency. On the contrary, the surge damping coefficient increases at longer periods and smaller amplitudes.

- Heave added mass coefficient is sensitive to oscillation periods at smaller amplitudes; on the other hand, quadratic heave damping tends to show minimal dependence on oscillation period, whereas it exhibits significant dependence with amplitude. The additional added mass is attributed to the strong viscous effects induced by the heave plates.

- The pitch damping coefficient exhibits similar behaviour as the heave damping coefficient. Pitch added mass moment of inertia is also higher than the potential-flow prediction, but interestingly shows the opposite dependence on motion amplitude compared to heave added mass.

In conclusion, the research gives an overall perspective of how the hydrodynamic characteristics vary with the characteristic parameters (amplitude and period), especially at extended periods. However, the work presented in this paper used a limited test matrix, and further analysis has to be carried out to generalise the results. One of the interesting prospects is to analyse the effect of the modified hydrodynamic parameters on the dynamic response of the FOWT. This study further encourages supplementing correction models to the pre-existing mid-fidelity hydrodynamic solvers based on potential flow theory with empirical damping or drag forces.

Acknowledgements

References

[1] Robertson A, Jonkman J, Masciola M, Song H, Goupee A, Coulling A, Luan C. Definition of the semisubmersible floating system for phase II of OC4. National Renewable Energy Lab.(NREL), Golden, CO (United States); 2014 Sep 1.

[2] Robertson AN, Wendt F, Jonkman JM, Popko W, Dagher H, Gueydon S, Qvist J, Vittori F, Azcona J, Uzunoglu E, Soares CG. OC5 project phase II: validation of global loads of the DeepCwind floating semisubmersible wind turbine. Energy Procedia. 2017 Oct 1;137:38-57.

[3] Wei YF, Yang JM, Chen X. A review of the hydrodynamic performance of heave damping plates on Spar platform. China Offshore Platform. 2010;25(6):1-4.

[4] Cozijn H, Uittenbogaard R, Brake ET. Heave, roll and pitch damping of a deepwater CALM buoy with a skirt. InThe Fifteenth International Offshore and Polar Engineering Conference 2005 Jun 19. OnePetro.

[5] Wadhwa H, Krishnamoorthy B, Thiagarajan KP. Variation of heave added mass and damping near seabed. InInternational Conference on Offshore Mechanics and Arctic Engineering 2010 Jan 1 (Vol. 49095, pp. 271-277).

[6] Lopez-Pavon C, Souto-Iglesias A. Hydrodynamic coefficients and pressure loads on heave plates for semi-submersible floating offshore wind turbines: A comparative analysis using large scale models. Renewable Energy. 2015 Sep 1;81:864-81.

[7] Nallayarasu S, Bairathi K. Hydrodynamic response of spar hulls with heave damping plate using simplified approach. Ships and Offshore Structures. 2014 Jul 4;9(4):418-32.

[8] Philip NT, Nallayarasu S, Bhattacharyya SK. Experimental investigation and CFD simulation of heave damping effects due to circular plates attached to spar hull. Ships and Offshore Structures. 2019 May 19;14(4):396-411.

CFD analysis of the semisubmersible

[9] Zhang S, Ishihara T. Numerical study of hydrodynamic coefficients of multiple heave plates by large eddy simulations with volume of fluid method. Ocean Engineering. 2018 Sep 1;163:583-98.

[10] Burmester S, Gueydon S, Vaz G, el Moctar B. Surge decay simulations of a semi-submersible floating offshore wind turbine. InProceedings of the 20th numerical towing tank symposium 2017 (pp. 2-3).

[11] Hirt CW, Nichols BD. Volume of fluid (VOF) method for the dynamics of free boundaries. Journal of computational physics. 1981 Jan 1;39(1):201-25.

[12] Rusche, H. Computational fluid dynamics of dispersed two-phase flows at high phase fractions Imperial College of Science, Technology Medicine, Department of Mechanical Engineering, 2002.

[13] Wang L, Robertson A, Jonkman J, Kim J, Shen ZR, Koop A, Borràs Nadal A, Shi W, Zeng X, Ransley E, Brown S. OC6 Phase Ia: CFD simulations of the free-decay motion of the DeepCwind semisubmersible. Energies. 2022 Jan;15(1):389.

[14] Robertson A, Bachynski EE, Gueydon S, Wendt F, Schünemann P. Total experimental uncertainty in hydrodynamic testing of a semisubmersible wind turbine, considering numerical propagation of systematic uncertainty. Ocean Engineering. 2020 Jan 1;195:106605.

[15] Li H, Bachynski-Polić EE. Experimental and numerically obtained low-frequency radiation characteristics of the OC5-DeepCwind semisubmersible. Ocean Engineering. 2021 Jul 15;232:109130.

[16] Sarpkaya T, Isaacson M, Wehausen JV. Mechanics of wave forces on offshore structures.

[17] Gao Z, Efthymiou M, Cheng L, Zhou T, Minguez M, Zhao W. Hydrodynamic damping of a circular cylinder at low KC: experiments and an associated model. Marine Structures. 2020 Jul 1;72:102777.

[18] Dütsch H, Durst F, Becker S, Lienhart H. Low-Reynolds-number flow around an oscillating circular cylinder at low Keulegan–Carpenter numbers. Journal of Fluid Mechanics. 1998 Apr;360:249-71.